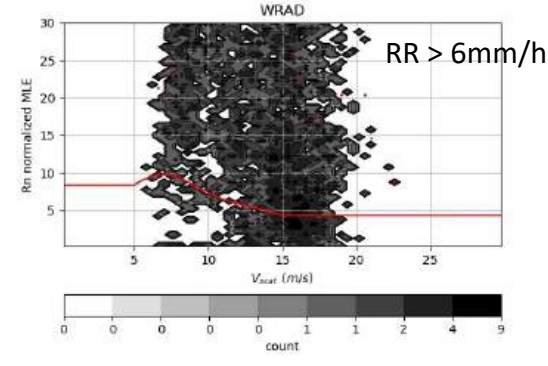
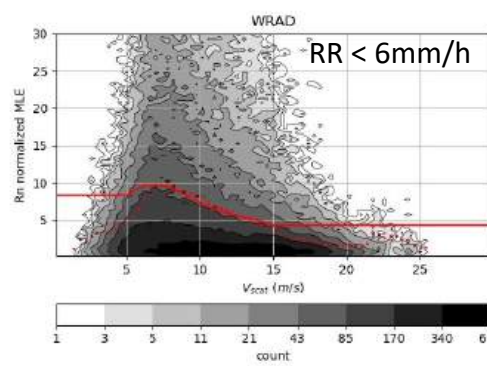
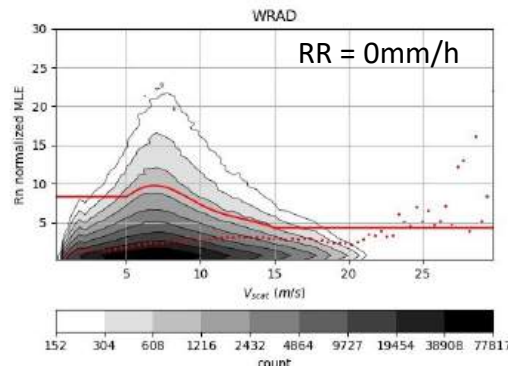
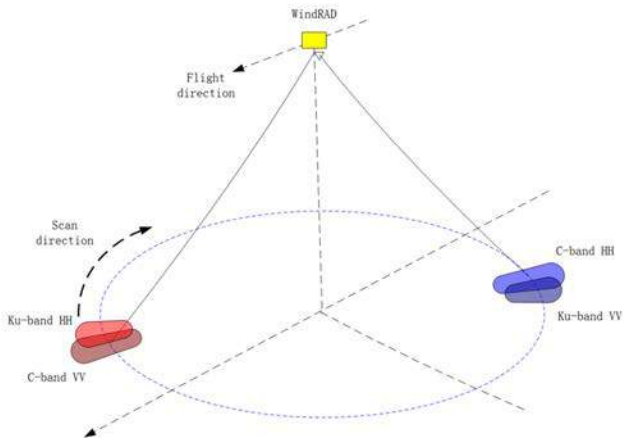


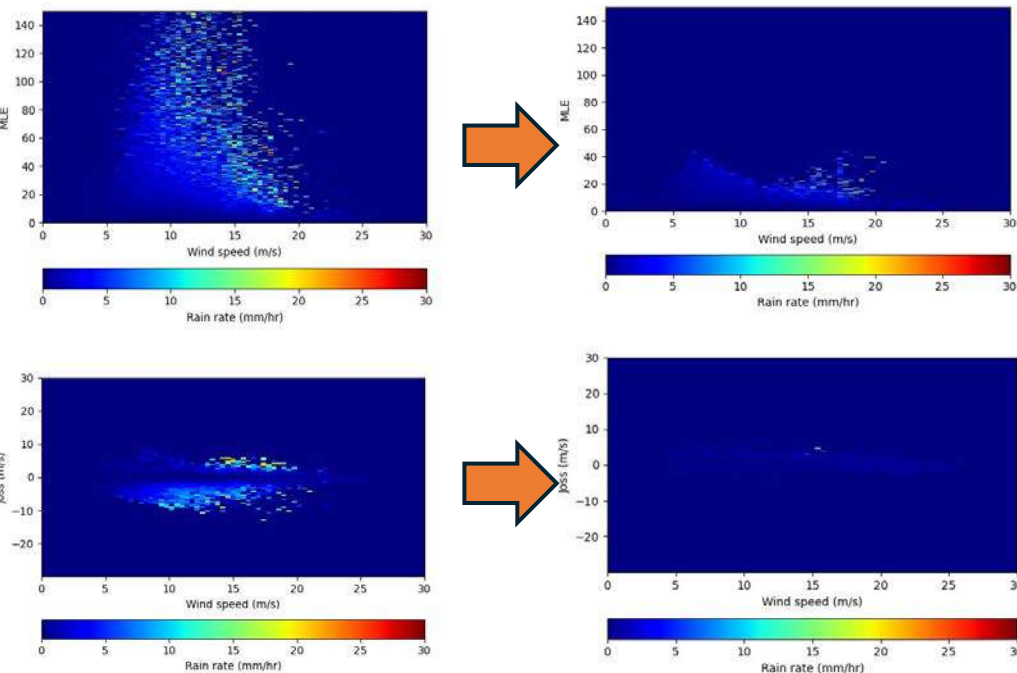
Quality Control of WindRAD Scatterometer

Zhen Li, Anton Verhoef, Ad Stoffelen
 Royal Netherlands Meteorological Institute

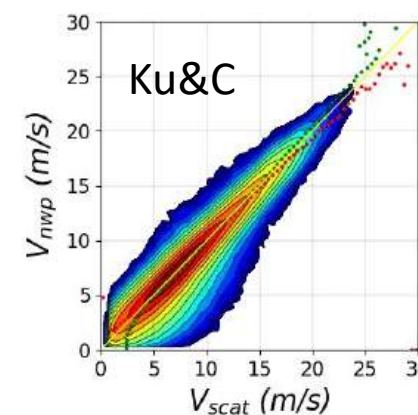
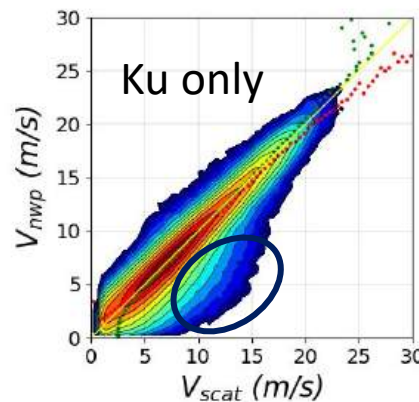


Rotating fan-beam with
 C- and Ku-band antennas

The classic QC method is based on the **MLE** (Maximum Likelihood Estimator).



Another method is **Joss**. Joss is defined as the analysis wind speed (wind field constructed in the ambiguity removal) minus the selected scatterometer wind. The WVCs with a Joss value lower than certain threshold are excluded.



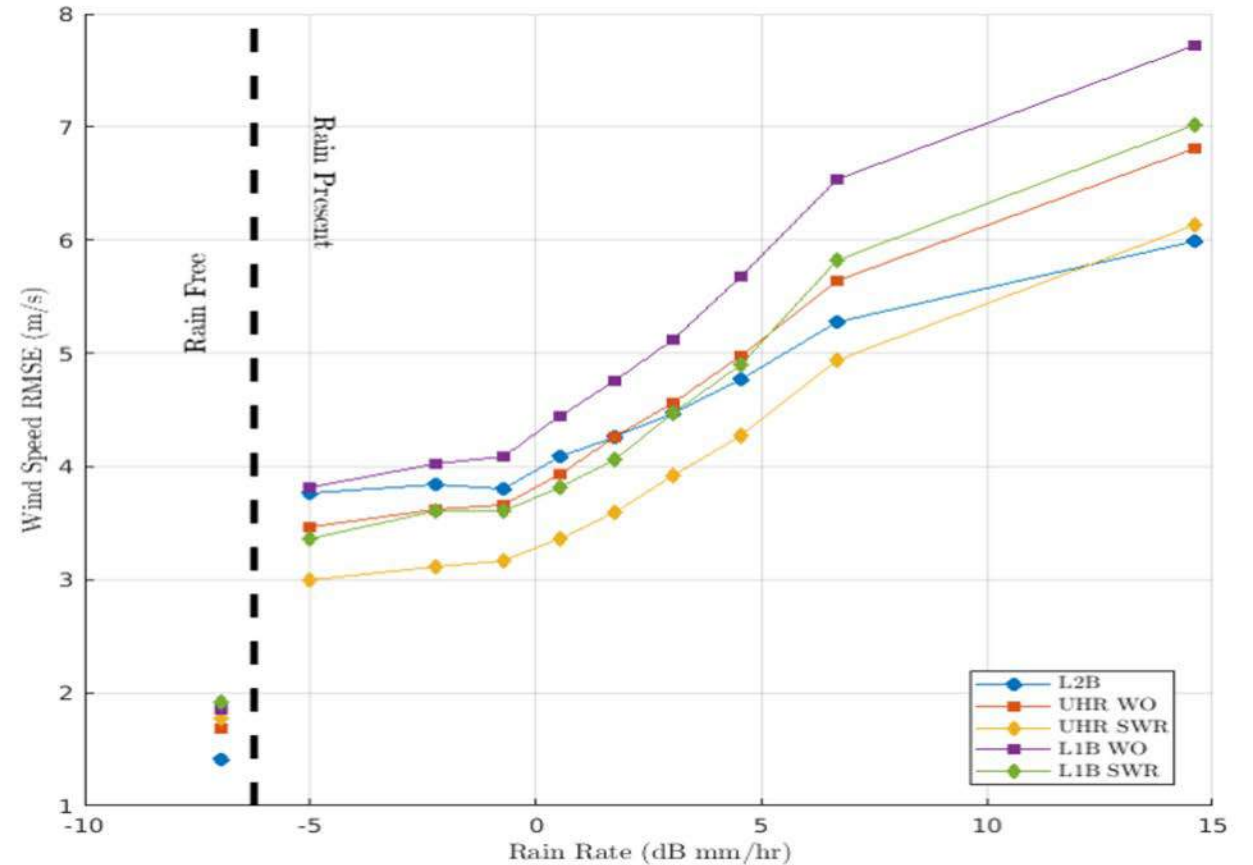
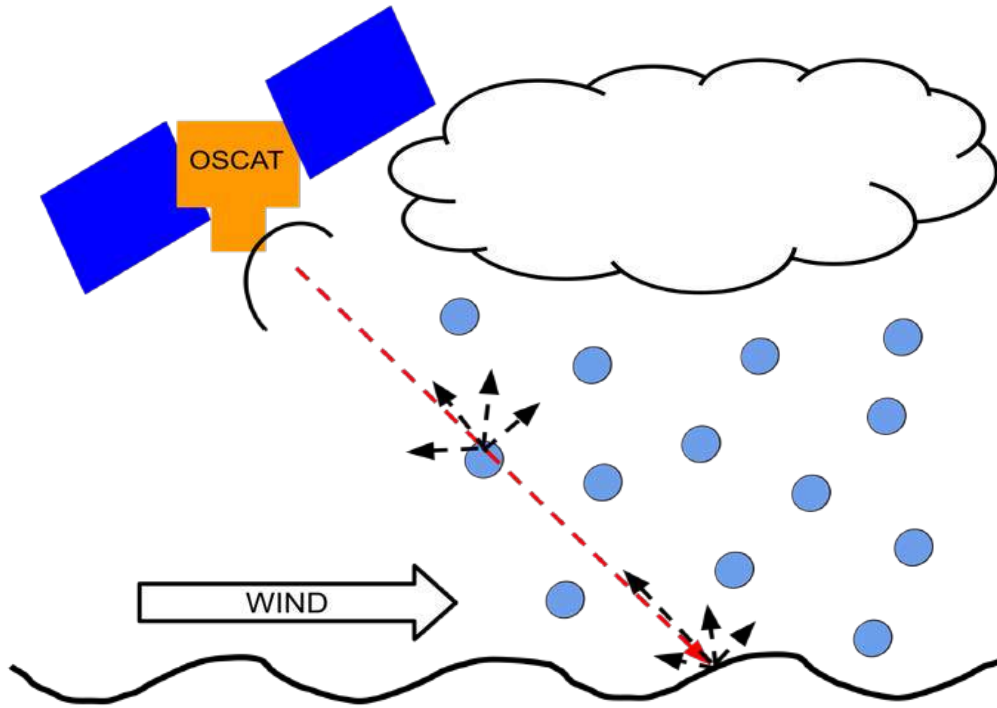
Impact study of scatterometer winds on heavy rain forecast in the JMA's regional forecast model

Yusuke Ioka (Japan Meteorological Agency)

Mitigating the Effects of Rain for OSCAT Wind Retrieval

Benjamin Fogg and David G. Long

Microwave Earth Remote Sensing Lab, Brigham Young University, Provo, UT





MAPPING ICE SLABS IN ANTARCTIC ICE SHELVES USING ENHANCED-RESOLUTION L- AND C-BAND RADAR BACKSCATTER IMAGE TIME SERIES

J. Z. Miller¹, D. G. Long², & R. Culberg³

¹Earth Science and Observation Center, CIRES, University of Colorado Boulder

²Department of Electrical and Computer Engineering, Brigham Young University

³Department of Earth and Atmospheric Sciences, Cornell University

email: jzmiller.research@gmail.com



Funded by:
NASA Cryospheric Sciences Program &
NASA SMAP Science Team



ABSTRACT

Enhanced-resolution radar backscatter (σ^0) image time series (2015) generated using observations collected by the short-lived (83 days) quad-polarization L-band radar (in scatterometer-mode) aboard the NASA Soil Moisture Active Passive (SMAP) mission and the vertically-polarized C-band Advanced SCATerometer (ASCAT) aboard the EUMETSAT Meteorological Operational (MetOp) satellite mission are exploited to map embedded ice structures -- including continuous meters-thick ice slabs, single or stacked sequences of thinner ice layers, and relatively sparse networks of ice pipes and lenses -- within the firm column of the percolation facies of Antarctic ice shelves (Figure 1). Combined, these satellite-derived parameters provide a continent-wide approximation of firm air depletion, which has implications for identifying ice shelves that are potentially vulnerable to supraglacial lake or firm aquifer formation, meltwater-induced hydrofracture, and collapse and disintegration from space. Distinctive spatial trends in L- and C-band σ^0 signatures identified via principal component analysis (PCA) are used to develop a multi-frequency polarimetric algorithm that is calibrated using firm cores, snow pits, and ground penetrating radar (GPR) transects (Figure 2). Algorithm results are partially validated using airborne ice-penetrating radar surveys (Figure 3) and optical and synthetic aperture radar (SAR) satellite imagery.

Ice slabs (~230,000 km²) are primarily mapped in the Antarctica Peninsula and in East Antarctica and preferentially form near ice shelf grounding zones extending from faster-flowing tributary glaciers. Scattered locations are also mapped in West Antarctica. Expansive ice slabs are mapped on the Scar Inlet, southern Larsen C, Larsen D, central George VI, northern Wilkins, Bach, Stange, southern Abbot, Shackleton, West, Amery, and Roi Baudouin ice shelves. On the Larsen C and D, Wilkins, and Abbot ice shelves, ice slabs overlay firm aquifers that have continuously existed within the deeper firm column for decades. Ice layers ~210,000 km² and ice pipes and lenses ~330,000 km² are mapped over the remainder of the percolation facies ~770,000 km² which covers ~50% of the total ice shelf extent. We attribute ice slab formation to enhanced surface melting driven by katabatic and foehn wind flow channeled downslope by the local topography. Heavy rainfall, extensive ice layering during sequential years, and brine infiltration within the firm column may precondition ice shelves for accelerated ice slab formation and/or expansion if Antarctica's climate continues to warm and seasonal surface melting increases in ex

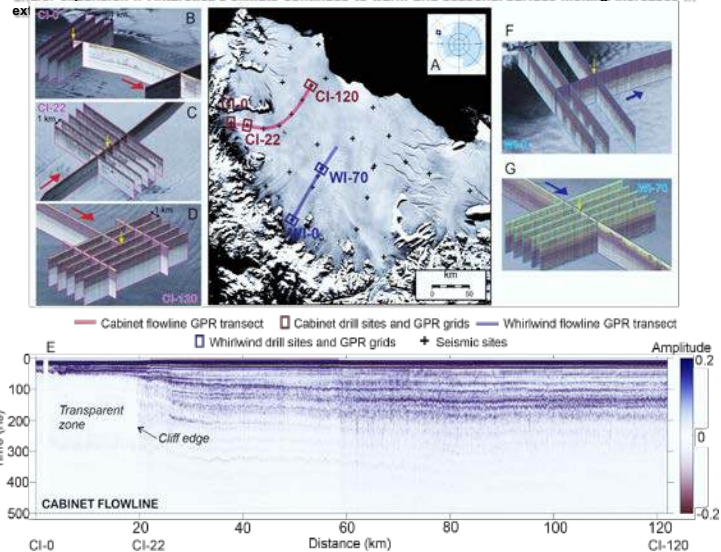


FIGURE 2. Ground Penetrating Radar (GPR) Transects

(A) Location map of Larsen C Ice Shelf on 2013-2014 MODIS Mosaic of Antarctic (MOA) image. The location map shows GPR, seismic and weather station sites. Boreholes were drilled at CI-0, CI-22, CI-120, WI-0 and WI-70. (B-D) Cabinet Inlet flowline dense GPR grids. (E) GPR transect along the Cabinet Inlet flowline. (F-G) Whirlwind Inlet flowline dense GPR grids. Yellow arrows (B-G) indicate respective drill site locations, and red (B-D) and blue (F-G) arrows respectively indicate ice flow directions in Cabinet and Whirlwind inlets.

Kulussa et al., submitted to Science.

Rapid formation of low-permeability ice slabs in Antarctic ice shelves.

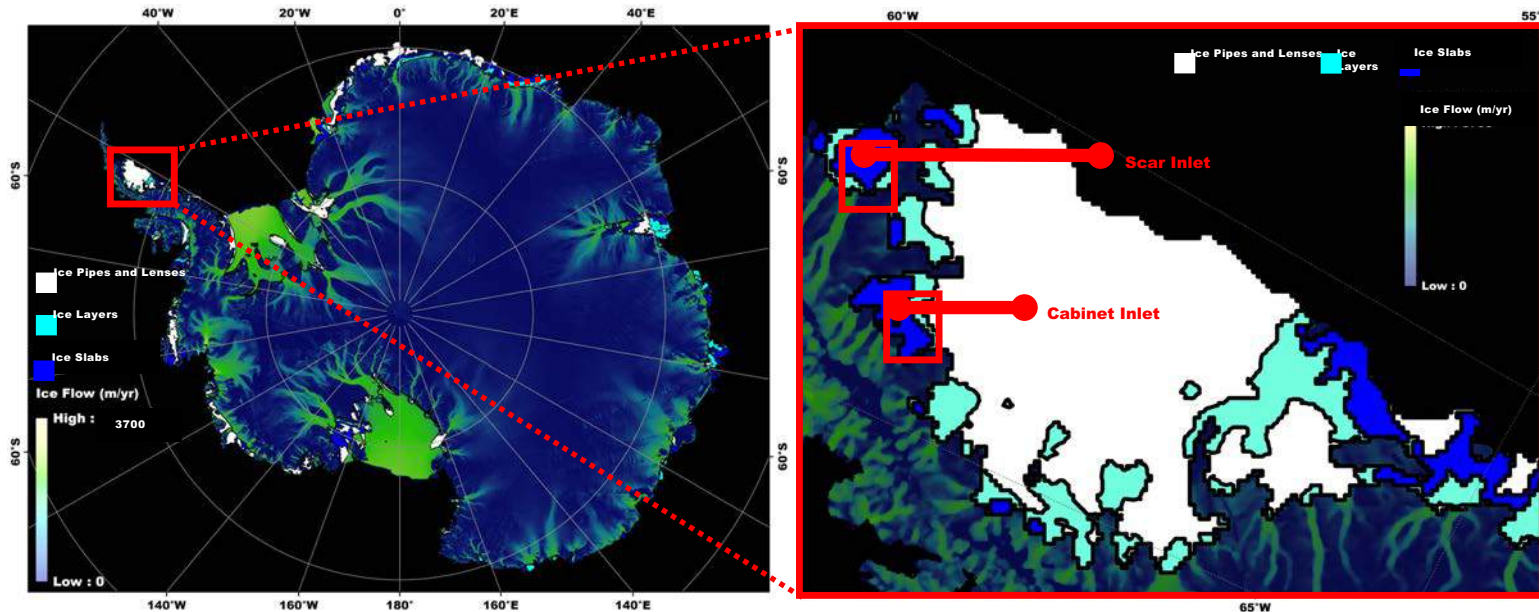


FIGURE 1. Mapping of Ice Slabs, Ice Layers, and Ice Pipes and Lenses using L- and C-band Radar Backscatter (2015)

Enhanced-resolution mapping generated using coincident σ^0 observations collected by the quad-polarization L-band radar (in scatterometer-mode) aboard the NASA SMAP satellite mission and the vertically polarized C-band ASCAT scatterometer aboard the EUMETSAT satellite mission over (left) Antarctica and (right) the Larsen C Ice Shelf. Airborne ice-penetrating radar surveys over the Cabinet and Scar inlets (red boxes) in the right image are shown in Figure 3. The black lines are the 2013-2014 MODIS MOA grounding lines and ice extent. The blue and green colored shading are ice

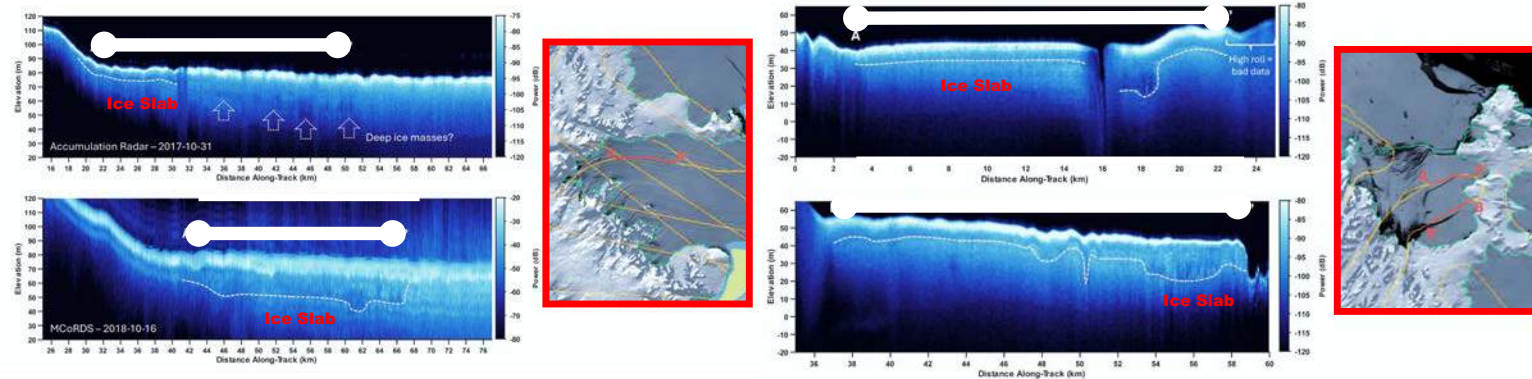


FIGURE 3. Airborne Ice-Penetrating Radar Surveys over the Cabinet and Scar Inlets

Airborne ice-penetrating radar surveys (Accumulation Radar and MCoRDS system) over ice slabs on (left) Cabinet and (right) Scar inlets. Yellow lines are flight lines overlaid the 2013-2014 MODIS MOA. The teal lines are the 2013-2014 MODIS MOA grounding lines and ice extent.

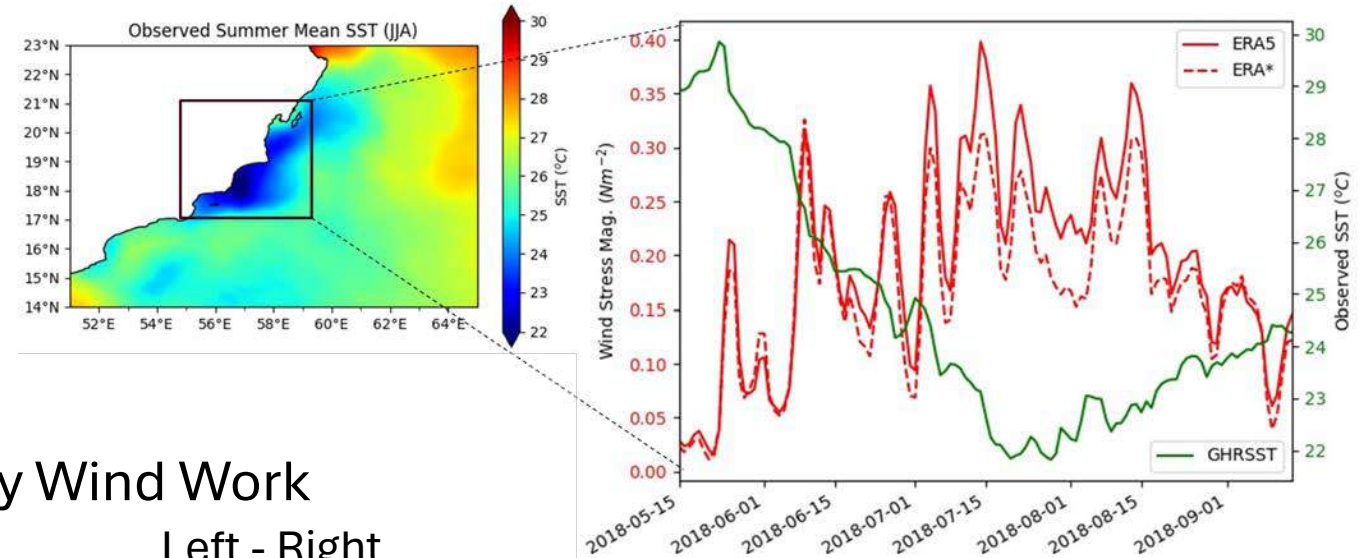
Modeling of a Coastal Upwelling Region using Scatterometer Based Bias Corrections of ERA5 Winds

Ethan E. Wright, Mark A. Bourassa

With support from Marcos Portabella and Eugenia Makarova

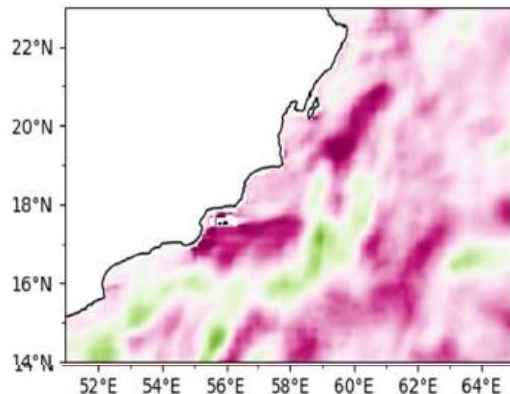
ERASTAR

A correction of ERA5 output by means of geo-located scatterometer-ERA5 differences over 3-day time windows. Produced through the ESA World Ocean Circulation project.

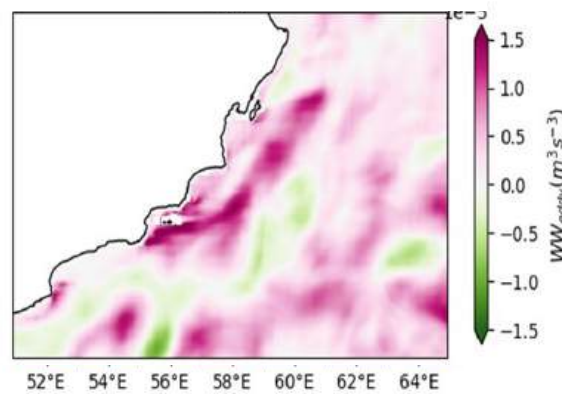


2018 Summer Mean (JJA) Eddy Wind Work

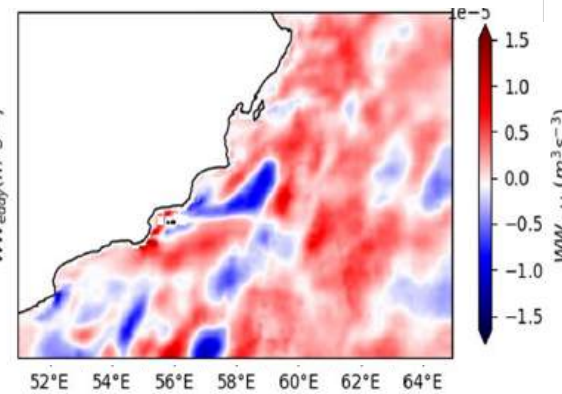
ROMS with ERAStar



ROMS with ERA5



Left - Right

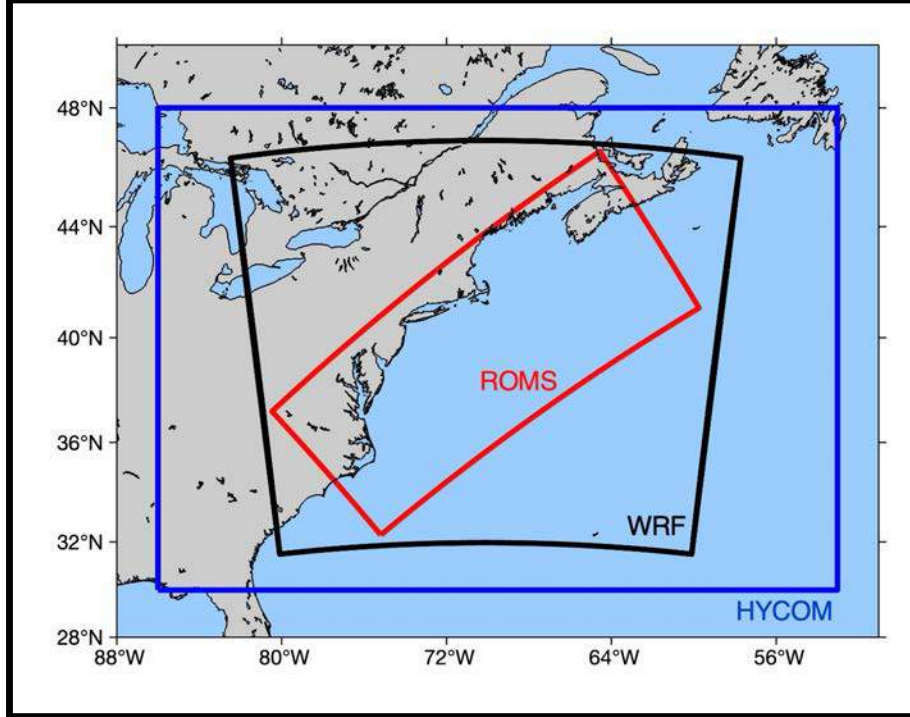


- Comparisons include the seasonal development of EKE and SST.

Integrating COARE 3.5 and Wind-Current Feedbacks into ROMS-WRF Coupling

L. Fernando Pareja-Roman, John Wilkin, Hernan Arango
 Department of Marine and Coastal Sciences, Rutgers University

ROMS, WRF and HYCOM (Data)



Relative wind speed

$$U_{air} = U_{wind} - U_{sur}$$

$$V_{air} = V_{wind} - V_{sur}$$

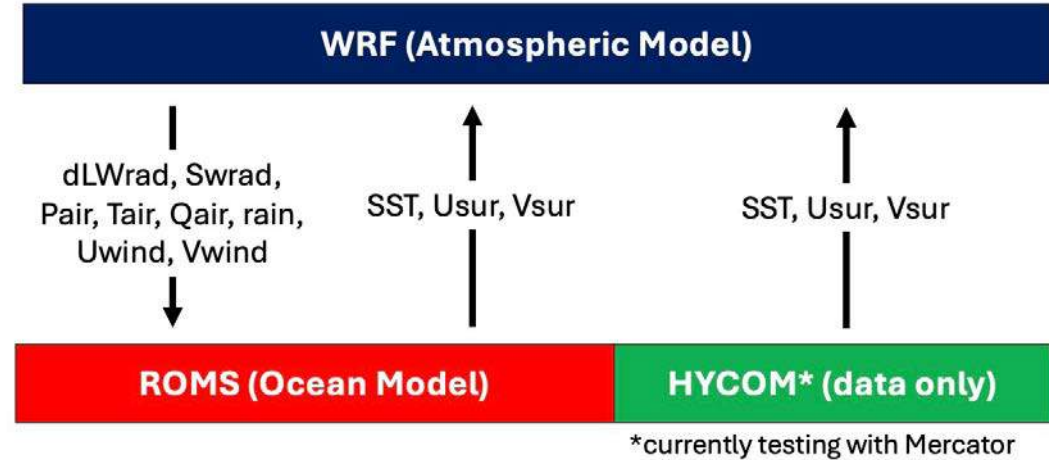
Gustiness-augmented speed

$$W_{mag} = \sqrt{U_{air}^2 + V_{air}^2}$$

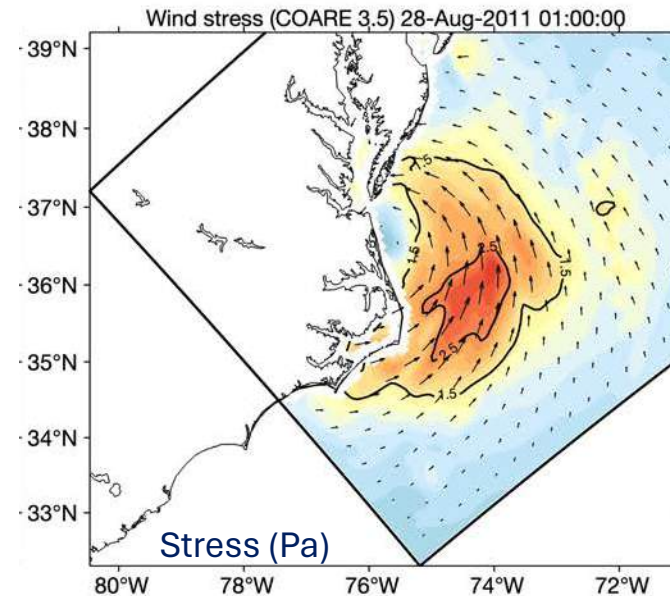
$$W_{speed} = \sqrt{U_{air}^2 + V_{air}^2 + W_{gus}^2}$$

Changes to Charnock alpha (v3.0 to v3.5)

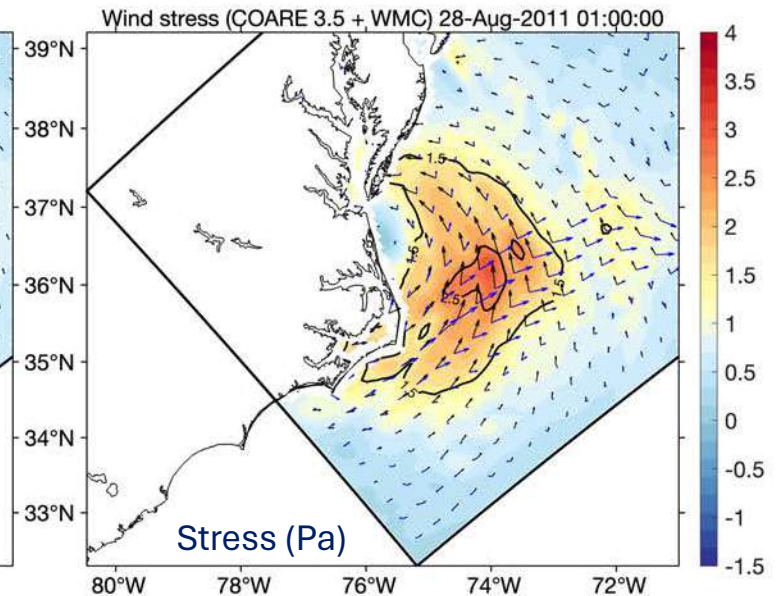
NUOPC/ESMF Coupling with non-matching model grids



COARE 3.5 No currents



COARE 3.5 With currents



Subsurface Temperature Anomalies off Central Oregon During 2014-2021

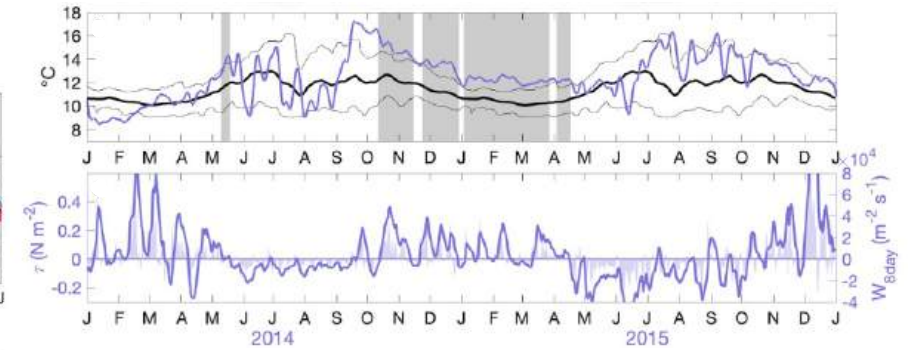
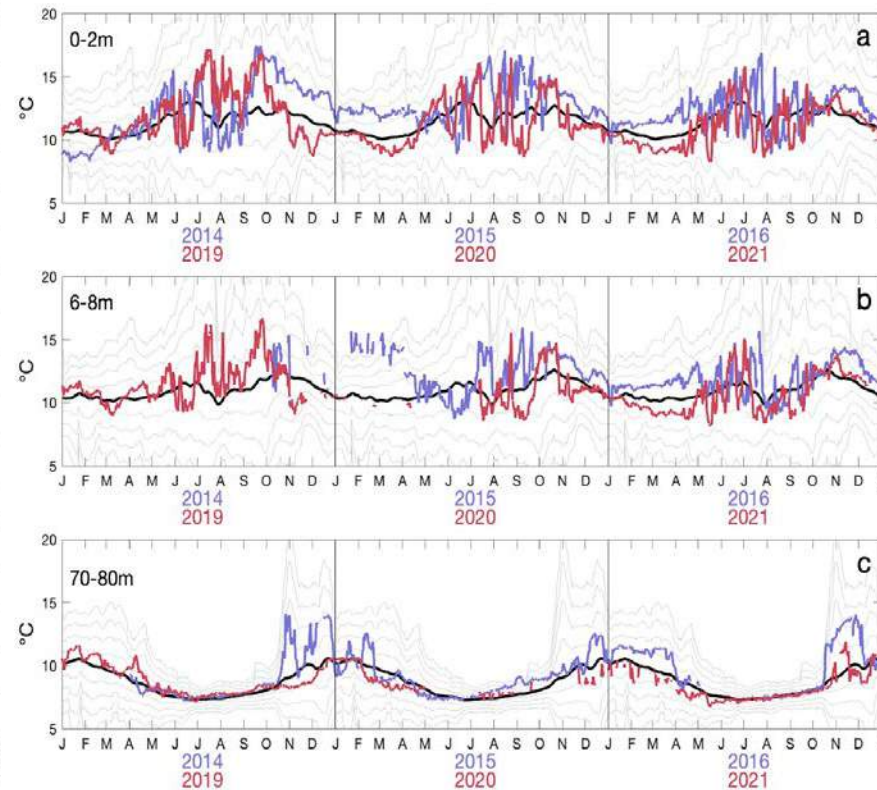
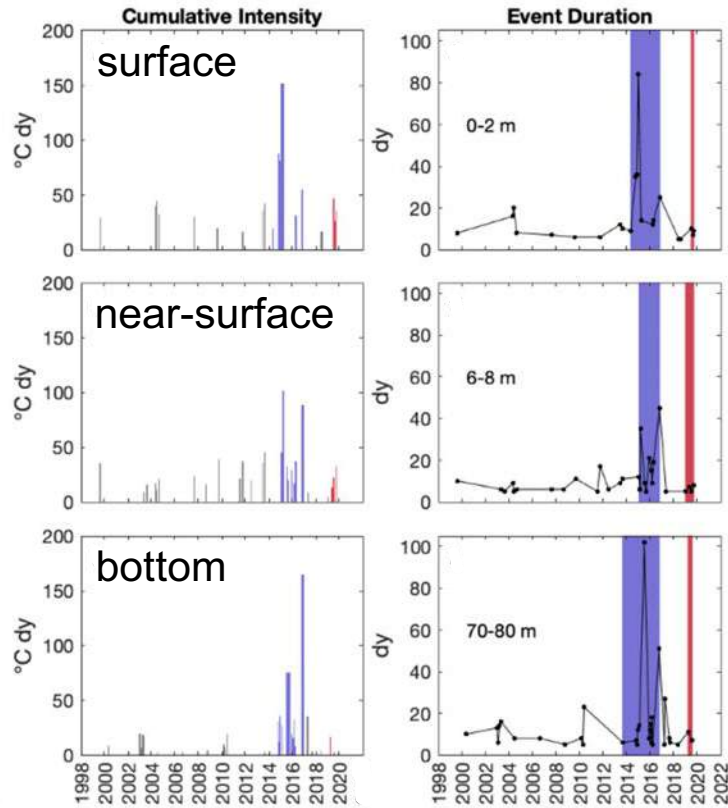
Brandy Cervantes, Melanie Fewings, Craig Risien

Oregon State University, College of Earth, Ocean and Atmospheric Sciences

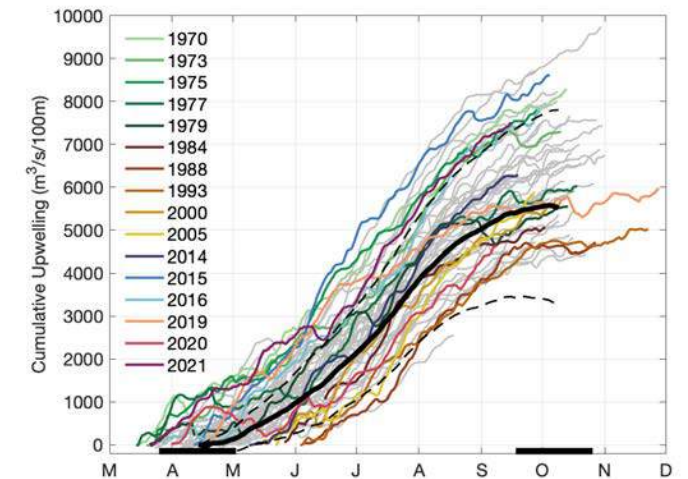
Increase in MHW characteristics from 1999-2021 varies by depth off central Oregon

The highest temperature anomaly in the 23-year time series was observed **near the bottom** in late 2016

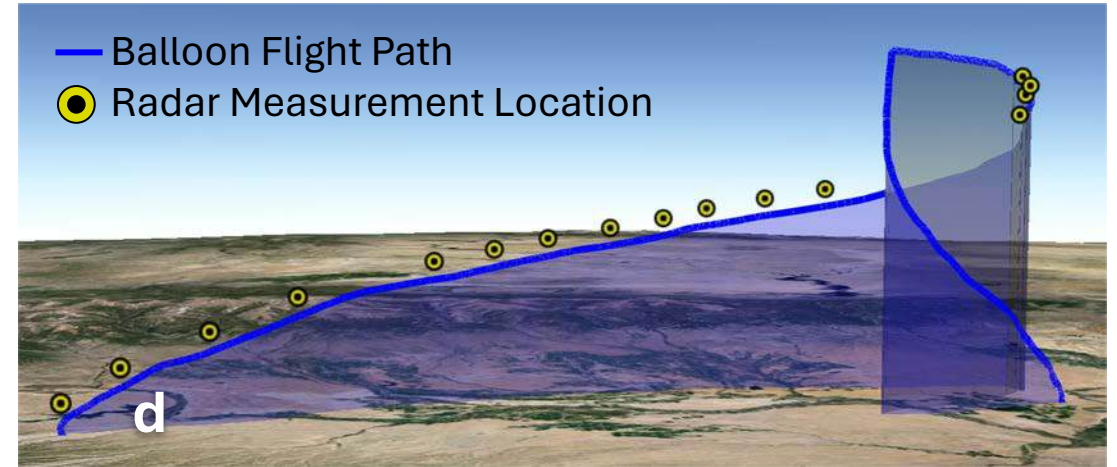
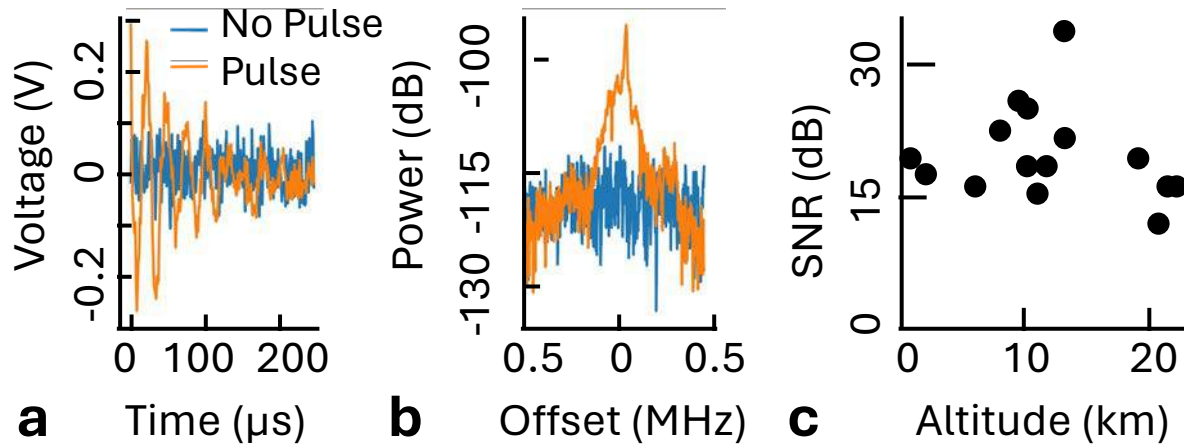
Upwelling winds interrupt MHWs and warming shortens upwelling season



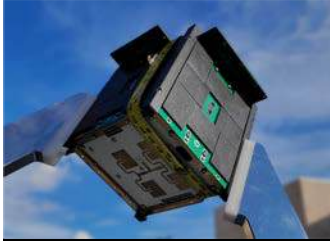
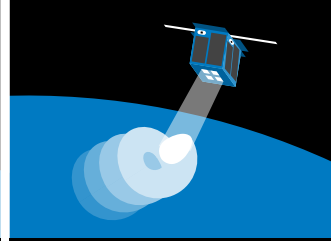



Variation in spring transition date relates to timing and severity of MHW



Veery Fledglings – Prototype Scatterometry from CubeSats



					
<input checked="" type="checkbox"/> V0.1 Launched 2021	<input type="checkbox"/> V0.2 Launched 2022	<input checked="" type="checkbox"/> V0.3, Launched 3/2024	<input type="checkbox"/> V0.4, Launching 10/2024	<input type="checkbox"/> V0.5 Launching 2025-H1	<input type="checkbox"/> V1.0 Launching 2026
Minimum Viable Satellite	Satellite Bus Improvements	Minimum Viable Radar	Wind Speed Radar	Prototype Scatterometer	Full-scale Scatterometer

Antarctica Ice Modeling for Cross-Calibration

$$\sigma_0 = 10 \log_{10} \left[\underbrace{AT(\theta_i)^2}_{\text{Volume backscatter}} \underbrace{\cos(\theta_i)}_{\text{Volume modulation}} \underbrace{M_v(\theta_a)}_{\text{Volume modulation}} + \underbrace{\sigma_s(\theta_i)}_{\text{Surface Backscatter}} \underbrace{M_s(\theta_a)}_{\text{Surface Modulation}} \right] + \mathbf{C}$$

Volume Component Surface Component
Volume backscatter Volume modulation Surface Backscatter Surface Modulation

